American Heart Association®

Metabolic Response to Stress by the Immature Right Ventricle Exposed to Chronic Pressure Overload

Masaki Kajimoto, MD, PhD; Muhammad Nuri, MD; Nancy G. Isern, MS; Isabelle Robillard-Frayne, MS; Christine Des Rosiers, PhD; Michael A. Portman, MD

Background—The right ventricle exposed to chronic pressure overload exhibits hypertrophy and decompensates when exposed to stress. We hypothesize that impaired ability to increase myocardial oxidative flux through pyruvate dehydrogenase leads to hypertrophied right ventricular (RV) dysfunction when exposed to hemodynamic stress, and pyruvate dehydrogenase stimulation can improve RV function.

Methods and Results—Infant male Yorkshire piglets (13.5±0.6 kg weight, n=19) were used to assess substrate fractional contribution to the citric acid cycle after sustained pulmonary artery banding (PAB). Carbon 13–labeled glucose, lactate, and leucine, oxidative substrate tracers for the citric acid cycle, were infused into the right coronary artery on 7 to 10 days after PAB. RV systolic pressure, RV free wall thickness, and individual cardiomyocyte cell size after PAB were significantly elevated compared with the sham group. Both fractional glucose and lactate oxidations in the PAB group were >2-fold higher than in the sham group. Pigs with overdrive atrial pacing (≈80% increase in heart rate) stress after PAB showed only a 22% increase in rate-pressure product from baseline before atrial pacing and limited carbohydrate oxidation rate in the right ventricle. Intracoronary infusion of dichloroacetate, a pyruvate dehydrogenase agonist, produced higher rate-pressure product (59% increase) in response to increased workload by atrial pacing in association with a marked increase in lactate oxidation.

Conclusions—The immature hypertrophied right ventricle shows limited ability to increase carbohydrate oxidation in response to tachycardia stress leading to energy supply/utilization imbalance and decreased systolic function. Enhanced pyruvate dehydrogenase activation by dichloroacetate increases energy supply and preserves hypertrophied RV contractile function during hemodynamic stress. (***J Am Heart Assoc***. 2019;8:e013169. DOI: 10.1161/JAHA.119.013169)

Key Words: congenital heart disease • myocardial metabolism • pressure overload • right ventricle

Right ventricular (RV) pressure overload occurs frequently in infants with congenital heart disease.[1–3] Obstruction to pulmonary flow, occurring with abnormalities such as pulmonary valve or arterial stenosis, yields chronic RV

pressure overload. Additionally, the right ventricle often persists as the systemic ventricle following palliation for complex defects. The immature right ventricle subjected to pressure overload exhibits maladaptive hypertrophy with diminished functional capacity.[4,5] Decreased RV function under these clinical scenarios in infants and children is most apparent when the heart is exposed to stressors such as tachycardia and hypoxia, as well as inflammation associated with cardiopulmonary bypass procedures.[6,7]

The mechanisms underlying RV dysfunction in these clinical scenarios still require elucidation to develop targeted interventions. Studies performed in vitro show that neonatal RV cardiomyocytes undergoing hypertrophy exhibit mitochondrial remodeling and hyperpolarization, which contribute to contractile dysfunction.[8,9] Dichloroacetate, a pyruvate dehydrogenase (PDH) kinase inhibitor,[10,11] reversed this hyperpolarization and has also been shown to improve contractile function assessed in hypertrophied right ventricle ex vivo. Although dichloroacetate is used clinically for other purposes,[12,13] translation of these studies to the bedside still requires evaluation in large animal models, which more

<div style="border: 2px solid red;">

Clinical Perspective

What Is New?

- The immature hypertrophied right ventricle exposed to stress shows an inability to increase substrate entry to the citric acid cycle through pyruvate dehydrogenase.
- Stimulation of pyruvate dehydrogenase flux by dichloroacetate reverses the metabolic defect, increases the substrate supply to the mitochondria, and preserves hypertrophied right ventricular contractile function during hemodynamic stress.

What Are the Clinical Implications?

- Metabolic manipulation, which improves substrate supply to the mitochondria, represents a potential pathway to improve function of the hypertrophied right ventricle in infants and children with congenital heart disease.

</div>

closely resemble clinical scenarios in infants and children with RV hypertrophy.

Dichloroacetate promotes PDH flux, suggesting that impairments in substrate oxidation are responsible for dysfunction of the hypertrophied right ventricle.[14–16] Few studies have directly evaluated substrate flux patterns within the immature right ventricle let alone in those exposed to sustained pressure overload. Our prior investigations performed in juvenile piglets showed that the nonhypertrophied right ventricle compared with the left ventricle possesses limited ability to change substrate flux in response to stresses including modulations in pressure loading.[17] This limited metabolic flexibility and inability to increase PDH flux during acute pressure overload by pulmonary artery banding (PAB) contributes to RV dysfunction.[18]

In summation, existing evidence supports a hypothesis that a metabolic impairment is responsible at least in part for dysfunction of the immature hypertrophied right ventricle exposed to stress. Additionally, established data implicate an inability to increase PDH flux as the primary metabolic abnormality.[14,18] First, we sought in our studies to test this hypothesis in an appropriate young animal model, which emulates clinically recognizable RV hypertrophy caused by pressure overloading in infants. We chose atrial pacing–induced tachycardia as the stressor in these studies because of ease of implementation in a complex experimental large animal model. Tachycardia, either sinus or supraventricular, frequently occurs in infants with RV hypertrophy caused by pressure overload and can cause RV dysfunction, and is thereby also clinically relevant.[19–21] Second, we then determined whether stimulation of PDH flux via dichloroacetate improved the RV functional response to atrial pacing–induced tachycardia in infant pigs. Finally,

we investigated whether other oxidative phosphorylation impairments, such as deficits in electron transport chain (ETC) enzymes, could occur with RV hypertrophy and impact functional reserve.

Methods

The data that support the findings of this study are available from the corresponding author upon reasonable request. Detailed methodology is provided in Data S1. The study was performed in accordance with the Guide for the Care and Use of Laboratory Animals, and all experimental procedures in this study were approved by Seattle Children's Institutional Animal Use and Care Committee.

### Animals and Experimental Design

A total of 19 infant male Yorkshire piglets (S&S Farms) were included in this study (Figure 1A and 1B). A minimum 7-day acclimation period after pig arrival was provided to minimize the stress associated with transportation. Animals were allotted to 1 of 2 protocols.

Protocol 1 served to assess the impact of PAB and RV hypertrophy on metabolic parameters. Pigs were randomized to either RV pressure overload for 7 to 10 days after PAB (PAB group, n=5) or a sham surgical procedure (sham group, n=4), which included thoracotomy but no PAB.

Protocol 2 served to evaluate the impact of dichloroacetate on the immature hypertrophied right ventricle during stress. In groups totally separate from protocol 1, pigs with PAB for 7 to 10 days were additionally exposed to hemodynamic stress by atrial overdrive pacing and randomized to receive either vehicle (phosphate-buffered saline) (stress group, n=5) or dichloroacetate (dichloroacetate group, n=5) into the right coronary artery.

Pig Model of Chronic RV Pressure Overload

All pigs were initially sedated with an intramuscular injection of ketamine (33 mg/kg) and xylazine (2 mg/kg), and were intubated with an endotracheal tube, facilitating mechanical ventilation and general anesthesia with inhaled isoflurane (1–3%). Heart and pulmonary artery (PA) were exposed through a small left lateral thoracotomy in the fourth or fifth intercostal space and partial pericardiotomy, and 2 pressure catheters (Millar Instruments, Inc) were inserted into the right ventricle and ascending aorta directly through the RV free wall and the aortic wall, respectively. After baseline hemodynamic and blood data were measured, a banding tape was placed around the main PA using a cotton umbilical tape ≈3 mm width (Ethicon). In the sham group, the banding tape was just looped around the PA without constriction. In the experimental (PAB) group, the banding tape was gradually constricted to
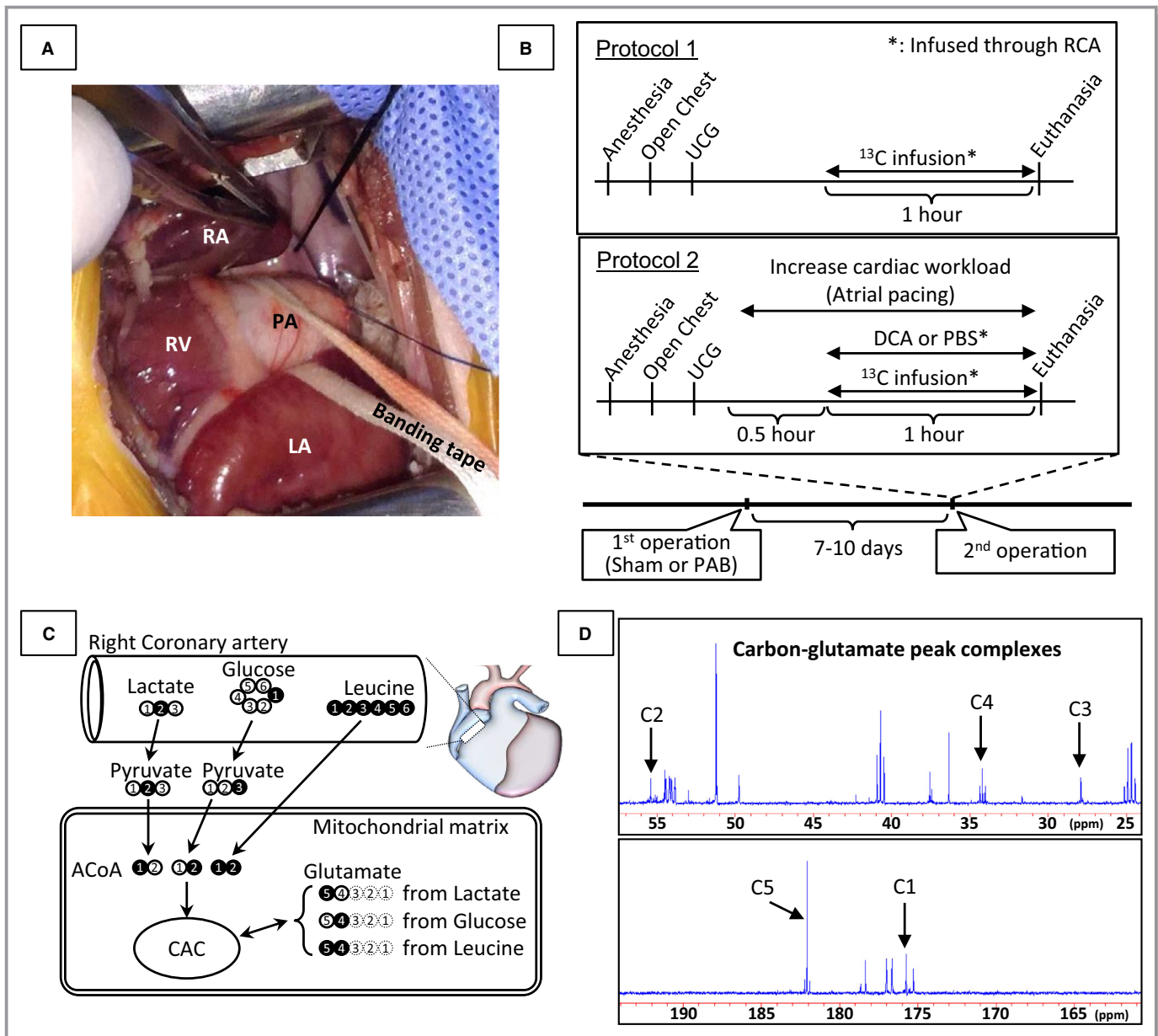
Figure 1. Experimental protocol. **A**, Pulmonary artery banding (PAB) via left thoracotomy. **B**, Study protocol. Pigs in the sham and PAB groups received ^{13}C-metabolic tracers at second operation, and pigs in the stress and dichloroacetate groups received atrial over pacing±dichloroacetate supplement in addition to ^{13}C-metabolic tracers. *Infused through the right coronary artery (RCA). **C**, Labeling patterns of acetyl coenzyme A and glutamate originating from metabolism of [2-^{13}C]lactate, [1-[13]C3]glucose and [U-[13]C6]leucine. The filled circle represents ^{13}C and the empty circle [12]C. **D**, Typical spectra for glutamates carbon 1–5 (C1–5). Chemical shifts in parts per million (ppm) were as follows: C3, 27.5; C4, 34.2; C2, 55.2; C1, 175.5; and C5 of glutamate, 182.1. ACoA indicates acetyl coenzyme A; CAC, citric acid cycle; LA, left atrium; PBS, phosphate-buffered saline; RA, right atrium; RV, right ventricle; UCG, ultrasound cardiography.

increase 2-fold of the baseline RV systolic pressure. A direct echocardiogram on the epicardium was performed for measurement of cardiac function, RV free wall thickness, and PA flow using an ultrasound machine (Sequoia C256; Siemens). Postoperative analgesia was administered for at least 72 hours, and animals were housed in a caged facility with full access to feed and water.

At 7 to 10 days postprocedure, the pigs were intubated through a surgical tracheostomy, mechanically ventilated with an oxygen (40–50%) and isoflurane (1–3%) mixture, and monitored with ECG and oxygen saturation. Pigs in both protocols then underwent median sternotomy and pericardiotomy and were allotted to 1 of the 2 protocols. Pigs allotted to protocol 1 then underwent infusion of isotopic

tracers into the right coronary artery as described below, and then the RV free walls were rapidly freeze-clamped and tissue extracted.

Pigs allotted to protocol 2 underwent additional procedures. Two epicardial pacing electrodes were placed into the right atrial myocardium and were connected to an external temporary dual-chamber pulse generator (Medtronic model 5345). Increased cardiac workload was induced by rapid right atrial pacing at a rate of ≈80% increase in baseline heart rate. After hemodynamic stabilization for ≈30 minutes, dichloroacetate or phosphate-buffered saline was infused through the right coronary artery for 60 minutes. Target intracoronary concentration of dichloroacetate was adjusted to 4 mmol/L. This concentration of dichloroacetate in our study is well within the range used by other investigators and based on the estimation method of Kudej used in an adult pig coronary ischemia model.[22]

^{13}C-Labeled Substrates

Labeled substrates in all protocols were infused from the right coronary artery through a directly inserted 24-gauge angiocatheter for the final 60 minutes of the protocol (Figure 1C). The intracoronary doses were adjusted to achieve 1.2 mmol/L [2-^{13}C]lactate, 2 mmol/L [1-^{13}C]glucose, and 2 mmol/L [U-^{13}C$_6$]leucine elevations in the right coronary artery and were based on the mean coronary artery flow per body weight calculated in our preliminary pig experiments.[23–25]

Nuclear Magnetic Resonance

Tissue processing was performed as previously described.[25,26] Nuclear magnetic resonance (^{13}C-NMR and ^{1}H-NMR) was performed on the RV extract tissue for measuring the fractional contribution (FC) of each substrate to the acetyl coenzyme A pool entering the citric acid cycle (CAC) and for measuring the concentration of myocardial energy metabolites, respectively, as previously described.[24,25,27–31] ^{13}C-NMR allows determination of the FC of labeled substrates via analyses of the ^{13}C-glutamate spectrum (Figure 1D) using the CAC analysis-fitting algorithm tcaCALC (kindly provided by the Advanced Imaging Research Center at the University of Texas, Southwestern). ^{1}H-NMR permits well-validated high-resolution and high-sensitivity analyses for quantitation of a robust number of metabolites including high-energy phosphates, such as phosphocreatine, ATP, ADP, and nicotinamide adenine dinucleotide (NADH).

Gas Chromatography Mass Spectrometry

Gas chromatography mass spectrometry (GCMS) was performed to measure the concentrations of CAC intermediates (citrate, α-ketoglutarate, succinate, fumarate, and malate),

pyruvate, lactate, and glutamate in RV tissue using Agilent 6890N gas chromatograph equipped with an HP-5 column coupled to a 5975N mass spectrometer (Agilent Technologies) as described elsewhere.[27]

Western Blot Analysis, Glycogen Assay, and Measurement of Blood Glucose and Plasma Triglyceride Levels

Protein was extracted from frozen RV tissue. The primary antibodies used in this study were 5′ AMP-activated protein kinase α, phospho–AMP-activated protein kinase–Thr172, acetyl coenzyme A carboxylase, phospho–acetyl coenzyme A carboxylase–Ser79, PDH, and phospho-PDH-E1α-Ser293 to evaluate the expression of key proteins regulating substrate oxidation as previously described (Table S1).[17,18,24,30,32] To assess the protein expression of ETC complexes, we also used the total oxidative phosphorylation rodent WB antibody cocktail (Abcam) that included specific subunits for each of the 5 ETC complexes. Commercially available kits were used to measure RV tissue glycogen concentration and plasma triglyceride (Cayman). Blood glucose was measured using a Bayer Contour point-of-care glucometer (Bayer HealthCare).

Histology

The fresh frozen RV free wall tissues were embedded in optimal cutting temperature compound in cryomolds. They were sectioned using a cryostat into 5-μm-thick slices and mounted onto slides. Wheat germ agglutinin staining was performed to measure cell size. Slides were stained for 10 minutes with Alexa Fluor 488-conjugated wheat germ agglutinin (1:200, Invitrogen) and Hoechst 33342 (1:1000, Invitrogen) at room temperature. Images were obtained using a digital fluorescence microscope (BZ-X700, Keyence) at a ×20 objective lens magnification and were analyzed by Fiji image software (an open source imaging program). The outline of myocytes was traced to determine myocyte cross-sectional area. A value was calculated by the measurements of 200 cells (from 3 nonoverlapping images randomly chosen for each slide) in an individual heart (2 slides for each animal). For the assessment of the extent of total myocardial fibrosis, slides were stained with Masson's trichrome (Polysciences Inc.) according to a standard protocol. In this staining, cytoplasm and muscle fibers stain red, whereas collagen fibers display blue coloration. Slide images were obtained using a digital microscope (BZ-X700, Keyence) at a ×4 objective lens magnification. Six nonoverlapping images were randomly chosen for analysis of each animal, and total myocardial fibrosis percentage was adjusted to a total tissue area in the analyzed image by Fiji. Phospho-PDH-E1α-Ser293 (1:500) was also used for immunohistochemical staining with

wheat germ agglutinin to confirm the activation effect of dichloroacetate to PDH flux.

Mitochondrial ETC Enzyme Activity

Enzymatic activities of the mitochondrial ETC complex I and II in the right ventricle were assessed using commercially available assay kits (Cayman Chemical) according to the manufacturer's instruction. For these reaction assays, 2 µg of isolated mitochondrial protein from the fresh frozen RV free wall tissues was loaded. Isolation of cardiac mitochondria was used by commercially available kits (Thermo Fisher Scientific).

Statistical Analysis

Reported values are expressed as means±standard error and/or median (interquartile range) in the text, figures, and tables. Statistical analysis was performed using PRISM 5.0 (GraphPad Software). For comparisons involving only 2 groups (sham versus PAB and stress versus dichloroacetate), the data were analyzed using 2-tailed Mann–Whitney U test. Paired, 2-tailed t test was used for the analysis of change from baseline data. The nonparametric Kruskal–Wallis test with Dunn's multiple comparison test was used for CAC intermediates and ETC data in all 4 groups. Criterion for significance was $P < 0.05$ for all comparisons.

Results

Mild-Moderate RV Pressure Overload by PAB Induced Hypertrophied Right Ventricle

There were no operative or technical complications in any piglets. Table 1 shows hemodynamic data in the sham and PAB groups at 7 to 10 days after the first procedure. Piglets in the PAB group had mild-moderate elevated RV systolic pressure, while RV end-diastolic pressure in the PAB group was unexpectedly similar to the sham group. The right ventricle in PAB group maintained cardiac workload assessed by rate-pressure product (RPP), calculated by (heart rate)× (peak systolic blood pressure)/1000 at baseline compared with sham, despite the elevated RV pressure. Doppler studies showed that surgical banding created a mild to moderate increase in RV pressure resulting in a measurable pressure gradient across the PAB site. Echocardiography confirmed that this fixed gradient over the protocol 1 (7–10 days after PAB) caused a modest but significant increase in RV wall thickness compared with normal hearts in the sham group (Table 1). As a result of rapid body weight increase in these young pigs, serial echocardiograms showed that percent change of RV wall thickness based on body weight decreased in the sham group but increased in PAB. Morphologic studies

with wheat germ agglutinin staining (Figure 2A) showed that the RV wall thickening resulted primarily from an increased cross-sectional area of individual cardiomyocytes, although the fibrotic area was also increased (Figure 2B). The hypertrophied right ventricle maintained cardiac workload assessed by RPP at baseline compared with the sham group, despite the elevated RV pressure (Table 1). Thus, the right ventricle exhibited hypertrophic changes with hemodynamic compensation.

Metabolism in the Immature Hypertrophied Right Ventricle

Concentrations for hemoglobin and specific metabolites, which could influence substrate metabolism, are shown in Table 2 for PAB and sham. GCMS showed that RV tissue levels for glutamate, pyruvate, and lactate were not different between the 2 groups. However, we found that PAB increased tissue levels for glycogen and its precursor uridine diphosphate–glucose measured by ^{1}H-NMR.

Table 1. Hemodynamic Data 7 to 10 Days After PAB

	Sham	PAB	P Value
BW, kg	15.5±0.9 15.9 (3.3)	16.1±0.6 16.2 (2.5)	0.71
Age, d	52±3 53 (10.5)	54±3 55 (14.5)	0.90
Temperature, °C	35.9±0.2 35.8 (0.8)	35.9±0.3 36.0 (1.2)	0.90
HR, beats per min	120±7 118 (29)	104±3 103 (13)	0.11
SP, mm Hg	71±2 71 (9)	80±4 78 (18)	0.11
RVSP, mm Hg	22±3 22 (11)	34±2 35 (6)	0.027
RVEDP, mm Hg	6±1 5 (3.5)	6±1 6 (1.5)	0.53
RV RPP, bpm×mm Hg/10^3	2.7±0.5 2.5 (1.8)	3.5±0.2 3.5 (0.6)	0.41
Echocardiogram			
RV-PA PG, mm Hg	5±3 3 (9)	29±4 30 (17)	0.016
RVWT, mm	3.6±0.2 3.6 (0.5)	4.7±0.1 4.7 (0.7)	0.036
% Change of RVWT/BW from baseline	−18.2±2.4 −18.3 (3.7)	30.6±5.2 27.4 (17.9)	0.029

Values are expressed as means±SE and median (interquartile range); n=4 to 5 per group. BW indicates body weight; HR, heart rate; RPP, rate-pressure product; RV, right ventricular; RVEDP, right ventricular end-diastolic pressure; RV-PA PG, pressure gradient between the right ventricle and the pulmonary artery; RVSP, right ventricular systolic blood pressure; RVWT, right ventricular free wall thickness; SP, systemic systolic blood pressure. *P* value: sham vs pulmonary artery banding (PAB).
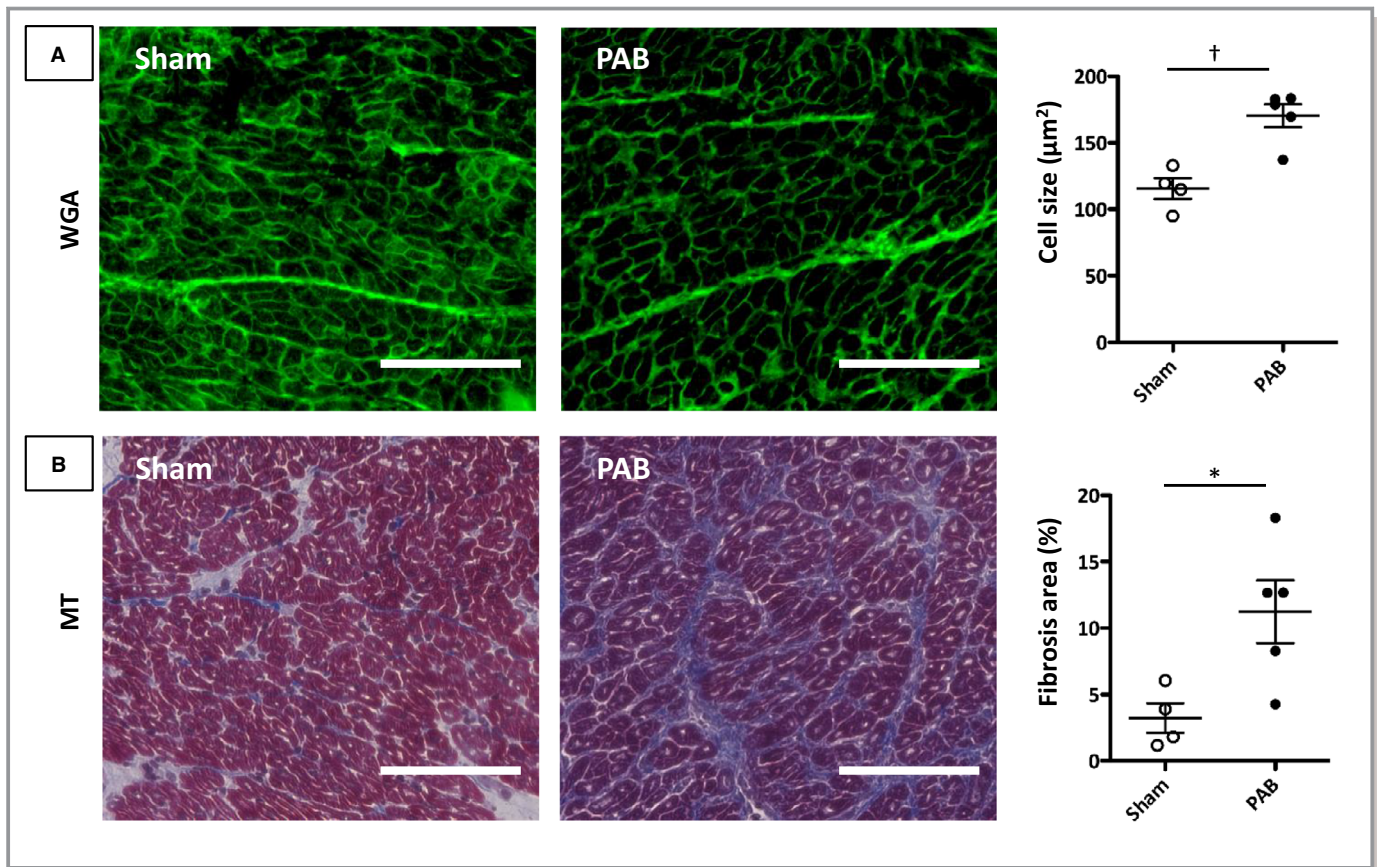
Figure 2. The hypertrophied right ventricle by pulmonary artery banding (PAB). **A**, Representative images of wheat germ agglutinin (WGA) staining and quantitative analyses of myocyte cross-sectional area. **B**, Masson's trichrome (MT) staining and quantitative analyses of myocardial fibrosis. Scale bar: 100 μm. Values are expressed as means±SE; n=4 to 5 per group. *$P<0.05$, †$P<0.01$ vs sham.

We determined ^{13}C-labeling of the glutamate pool using NMR spectroscopy on RV tissue extracts. Representative NMR spectra in Figure 3A illustrate the more obvious differences in ^{13}C-labeling patterns during baseline conditions for PAB and sham. Carbon 5 glutamate spectra demonstrate a larger singlet to doublet area ratio in PAB. FC of ^{13}C-labeled substrates supplied to the right ventricle determined using the tcaCALC program are shown in Figure 3B. In both the PAB and sham groups, FC-lactate predominates over FC-glucose as the principal carbohydrate source undergoing oxidation. Although both carbohydrate FCs are elevated in PAB over sham, only the marked increased in FC-lactate is significant. Differences in FC-carbohydrate could not be attributed to differences in RV tissue branched-chain amino acid (leucine) contribution is not altered by PAB. Parallel to the increase in FC-carbohydrates, contribution from unlabeled substrates is markedly lower in PAB. Carbohydrates are metabolized and contribute reducing equivalents to the CAC via PDH. Accordingly, we also evaluated expression and activity of select enzymes, which regulate flux through PDH. We measured protein expression levels of phospho-PDH (an inactive form of PDH) and total PDH (Figure 3C). These 2 proteins in PAB were lower than in sham, but the difference in phospho-PDH did not achieve significance (P=0.06). The phospho-PDH relative to total PDH was also not significantly different. The phosphorylation state and content for acetyl coenzyme A carboxylase and AMP-activated protein kinase, pivotal enzymes regulating metabolic flux, were also not impacted by PAB.

Energy Metabolism in the Immature Hypertrophied Right Ventricle

We used ^{1}H-NMR to determine whether adaptations in substrate oxidation yielded concomitant changes in high energy phosphate balance. Figure 4A illustrates representative ^{1}H-NMR spectrum. Chemical shifts detected for metabolites by ^{1}H-NMR are documented in Data S1. First, RV [phosphocreatine]/[ATP] and [ATP]/[ADP] did not differ significantly between PAB and sham, but [NADH]/[NAD$^+$] was significantly lower in PAB. [NAD$^+$] and [NADH] were normalized relative to the total creatine content (creatine+[phosphocreatine]), revealing that [NAD] was higher in PAB (Figure 4B).

Table 2. Metabolite Data 7 to 10 Days After PAB

	Sham	PAB	P Value
Blood or plasma			
Hemoglobin, g/dL	7.9±0.2 7.9 (0.8)	8.5±0.4 8.9 (1.9)	0.56
Glucose, mg/dL	143±42 140 (158)	164±49 161 (190)	0.89
Triglycerides, mg/dL	15.4±4.4 11.4 (13.8)	16.5±2.1 15.6 (8.3)	0.41
RV tissue			
Glutamate, nmol/mg	4.1±0.6 4.3 (2.3)	4.2±0.2 4.1 (0.9)	0.73
Pyruvate, nmol/g	115±33 102 (121)	135±24 111 (99)	0.56
Lactate, mmol/g	2.9±0.5 3.0 (1.8)	2.0±0.2 1.9 (0.8)	0.29
Glycogen, μg/mg protein	23.4±4.3 22.6 (16.3)	38.2±4.3 39.4 (14.4)	0.064
UDP-glucose, AU*	0.0004±0.0001 0.0004 (0.0003)	0.0020±0.0002 0.0021 (0.0008)	0.036

Values are expressed as means±SE and median (interquartile range); n=4 to 5 per group. *P* value: sham vs pulmonary artery banding (PAB). AU indicates arbitrary units; RV, right ventricular.

*Uridine diphosphate (UDP)-glucose was measured by ^{1}H-nuclear magnetic resonance and normalized relative to the total creatine content (creatine+[phosphocreatine]).

Hemodynamic Stress by Rapid Atrial Pacing and Intracoronary Dichloroacetate Infusion

In a separate protocol, we then assessed hemodynamic function and energy metabolism in the hypertrophied right ventricle during stress induced by rapid pacing and the efficacy of metabolic modulation by intracoronary infusion of dichloroacetate. Baseline parameters were similar between groups (Table 3). Rapid atrial pacing resulted in a decrease in RV systolic pressure with only a modest increase (≈20%) from baseline in RV RPP in the stress group. Dichloroacetate, provided to right ventricles with similar baseline hemodynamics, significantly amplified the RV RPP response (≈60% increase) to atrial pacing compared with the stress group. This result on RV RPP was also recognized in the relative change data between the end of the 30 minutes of hemodynamic stabilization just before dichloroacetate infusion (shown as pacing) and end point. Both RV and left ventricular (LV) RPP had similar competency during rapid pacing stress in the dichloroacetate group, whereas RPP in the stress group was significantly lower in the right ventricle than the left ventricle (*P*=0.041). Additionally, dichloroacetate maintained RV developed pressure, calculated by (RV systolic pressure−RV end-diastolic pressure), during pacing stress.

Dichloroacetate Modulation of Metabolism

Dichloroacetate, as expected, induced marked dephosphorylation of PDH compared with stress, consistent with inhibition of PDH kinase and activation of PDH. This dichloroacetate effect was apparent on fluorescent staining and immunoblot (Figure 5A and 5B). Accordingly, ^{13}C-NMR spectra demonstrate a large singlet relative to doublet in the dichloroacetate compared with stress (Figure 5C), consistent with a greater fractional lactate contribution via PDH. Analyses by tcaCALC (Figure 5D) confirmed that FC-lactate was substantially greater in the dichloroacetate group (46.6±7.7%) compared with the stress group (6.1±1., *P*=0.008). Concomitantly, tissue lactate level measured by GCMS was lower in the dichloroacetate group (Figure 5E). Consistent with the marked increase lactate oxidation, which also converts [NAD$^+$] to [NADH], dichloroacetate elevated [NADH]/[NAD$^+$], although there was no difference in [phosphocreatine]/[ATP] or [ATP]/[ADP] (Figure 5F).

CAC Intermediates

We used GCMS to determine absolute concentrations of CAC intermediates. PAB alone, although inducing a shift towards carbohydrate oxidation, did not alter these CAC levels in the immature right ventricle (Figure 6A and 6B). However, stress tachycardia resulted in accumulation of total CAC intermediates, and specifically citrate and α-ketoglutarate, thereby suggesting the existence of a metabolic block in the CAC pathway to succinate. Right ventricles receiving dichloroacetate provided during pacing showed reversal of these accumulations (Figure 6A and 6B).

ETC Activity

The [NADH]/[NAD$^+$] can depend on flux through the ETC. We performed immunoblots to determine enzyme expression, and separately conducted activity assays in isolated mitochondria. Immunoblots demonstrated that the hypertrophied right ventricle did not induce a change in expression for ETC complexes (ETC complex III was not detected by immunoblots) (Figure 6C). However, the hypertrophied right ventricle by PAB induced a significant decrease in ETC complex II, although not ETC complex I activity (Figure 6D and Figure S1). Dichloroacetate had no impact on ETC activity.

Discussion

We sought to determine whether limitations in PDH flux impair the ability of the immature and hypertrophied right ventricle to functionally adapt to stress. Studies in several experimental animal models indicate that LV hypertrophy,
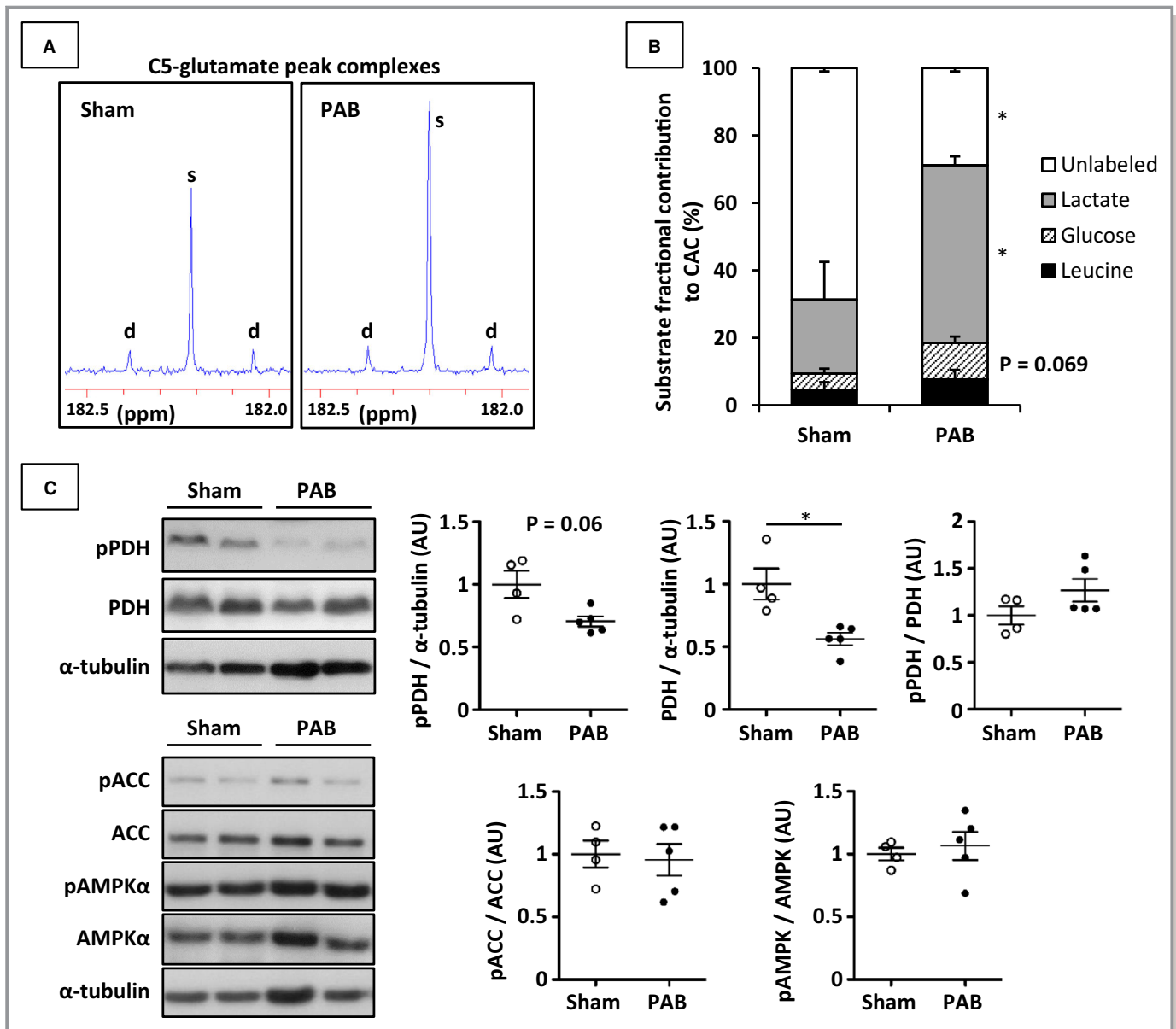
Figure 3. Metabolic alternations by chronic right ventricular pressure overload. **A**, Representative spectra for C5-glutamates. C5-glutamate in the pulmonary artery banding (PAB) group shows increased singlet peak area (s) relative to doublet spike areas (d), indicating increased lactate contribution compared with the sham group. **B**, Substrate fractional contributions to acetyl coenzyme A were analyzed by ^{13}C-nuclear magnetic resonance. PAB prominently increased lactate oxidation compared with sham at the end of protocol. **C**, Representative immunoblots data and the pooled data. ACC indicates acetyl coenzyme A carboxylase; AMPKα, 5′ AMP-activated protein kinase α; AU, arbitrary unit; pACC, phospho-acetyl coenzyme A carboxylase; pAMPKα, phospho-5′ AMP-activated protein kinase α; PDH, pyruvate dehydrogenase; pPDH, phospho-pyruvate dehydrogenase. Values are expressed as means±SE; n=4 to 5 per group. *$P<0.05$ vs sham.

caused by pressure overload, induces a shift from fatty acid to carbohydrate oxidation.[33,34] The immature right ventricle in our experiments responds in a similar manner during baseline conditions without workload stimulation. The shift is evident mainly from the marked increase in FC from lactate, which is the predominant carbohydrate used by immature myocardium.[35,36] Lactate metabolizes to pyruvate via the lactate dehydrogenase and then enters the CAC through PDH. The

relative increase in flux through PDH accompanies stabilization in myocardial oxygen consumption, assumed as no significant difference occurred in RPP between sham and PAB.

The mechanisms responsible for promoting PDH flux with the immature hypertrophied right ventricle remain unclear and may differ from those apparent in the left ventricle. Content and the phosphorylation state of at least 3 key enzymes involved in the regulation of substrate oxidation, PDH, acetyl
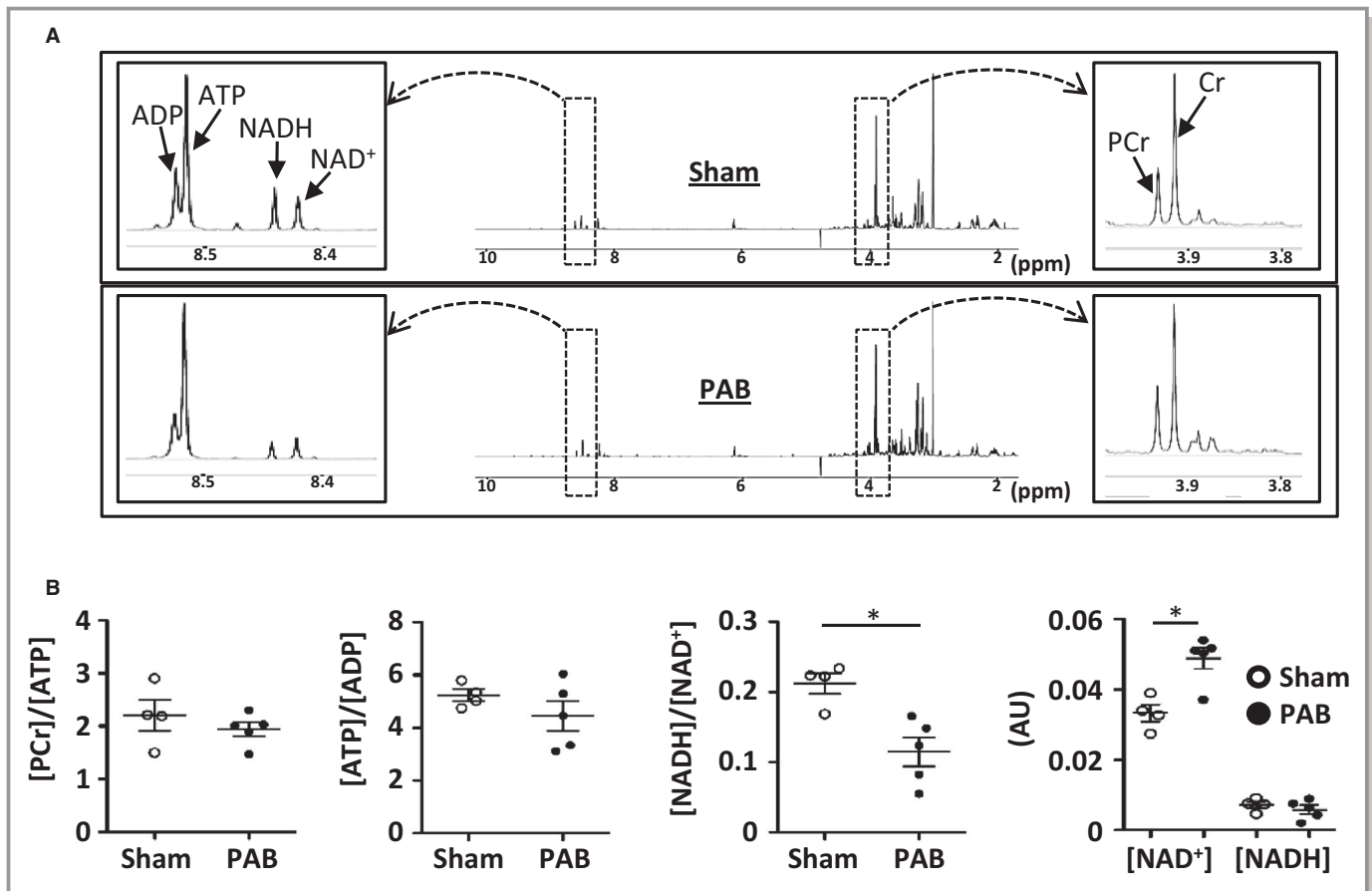
Figure 4. Right ventricular (RV) energy metabolites under chronic RV pressure overload. **A**, Typical ^{1}H-nuclear magnetic resonance spectrum for energy metabolites. **B**, RV[phosphocreatine (PCr)]/[ATP] and [ATP]/[ADP] were similar between the 2 groups. Pulmonary artery banding (PAB) demonstrated significantly lower [nicotinamide adenine dinucleotide (NADH)]/[oxidized form of nicotinamide adenine dinucleotide (NAD$^+$)] than sham. This was based on the difference of [NAD$^+$]. AU indicates arbitrary units. Values are expressed as means±SE; n=4 to 5 per group. *P<0.05 vs sham.

coenzyme A carboxylase, and AMP-activated protein kinase, do not change in a manner consistent with this shift. The immunoblot data indicate that PDH-E1α phosphorylation, considered a principal regulatory mechanism for this enzyme, does not seem to participate in the modulation of these substrate oxidation shifts in our experimental model. However, the overall content of PDH-E1α does decrease with hypertrophied right ventricle, possibly impairing the ability to modulate activity with changes in work demand. Mitochondrial [NADH] also regulates PDH by allosteric inactivation.[37] Accordingly, we observed a significant decrease in [NADH]/ [NAD$^+$], which theoretically could promote an increase in PDH flux. This observation poses difficulties for interpretation as our [NADH]/[NAD$^+$] values were obtained from whole tissue and represent composites from cytosolic and mitochondrial compartments. The intercompartmental issue is more complex as increased lactate oxidation, observed with hypertrophied right ventricle, would be expected to increase the reduction of [NAD$^+$], leading to accumulation of [NADH] in the

cytosolic compartment. Prior studies have shown that LV hypertrophy induced by pressure loading modifies capacity and kinetic regulation of the carriers responsible for shuttling, reducing equivalents from the cytosol to the mitochondria.[38,39] Theoretically, our observations, related to shifts in both substrate oxidation and [NADH]/[NAD$^+$], could result from hypertrophied RV-induced changes in shuttle capacities. Additionally, or alternatively, we observed a decrease in ETC complex II capacity, suggesting that a mitochondrial deficit induced by RV remodeling during hypertrophy plays a role in altering the [NADH] redox state.

Although the functional capacity of the immature hypertrophied right ventricle appears unaltered under our experimental baseline conditions, application of stress through rapid pacing reveals some functional abnormalities. In this maladaptive state, the right ventricle fails to achieve the RPP attained with rapid pacing and dichloroacetate. Additionally, unlike RV RPP response with dichloroacetate, RV RPP does not increase in synchronization with LV RPP in stress. Overall,

Table 3. Hemodynamic Data at Baseline Before Pacing Stress, at the End of 30-Minute Stabilization After Pacing, and at End Point

	Baseline (T1)		Pacing (T2)		End Point (T3)		Relative Change Between T1 and T3		Relative Change Between T2 and T3	
	Stress	Dichloroacetate	Stress	Dichloroacetate	Stress	Dichloroacetate	Stress	Dichloroacetate	Stress	Dichloroacetate
HR, beats per min	116±6 125 (26)	105±2 105 (9)	187±4 186 (14)	180±9 185 (37)	192±4 188 (15)	187±6 187 (25)	1.67±0.10 1.59 (0.45)	1.79±0.08 1.78 (0.34)	1.03±0.02 1.01 (0.06)	1.05±0.05 1.00 (0.16)
RV SP, mm Hg	36±5 30 (20)	33±3 32 (10)	30±4 28 (17)	29±1 28 (6)	26±3 26 (14)	29±3 27 (8)	0.74±0.04 0.71 (0.13)	0.88±0.06 0.88 (0.22)	0.88±0.02 0.88 (0.07)	1.01±0.04* 1.00 (0.17)
RVEDP, mm Hg	6±1 6 (1.5)	7±1 7 (3.5)	7±1 7 (1.5)	8±1 8 (2.0)	7±1 7 (2.5)	8±1 8 (1.5)	1.11±0.11 1.17 (0.50)	1.19±0.09 1.14 (0.34)	1.00±0.08 1.00 (0.29)	0.98±0.02 1.00 (0.05)
RV RPP, beats per min×mm Hg/10³	4.2±0.7 3.7 (3.1)	3.5±0.2 3.5 (0.8)	5.5±0.7 5.3 (2.8)	5.2±0.4 4.8 (1.3)	5.0±0.6 4.9 (2.6)	5.5±0.6 5.0 (2.1)	1.22±0.07 1.32 (0.26)	1.59±0.14* 1.58 (0.61)	0.91±0.02 0.91 (0.10)	1.05±0.05* 1.04 (0.22)
RV DevP, mm Hg	29±5 24 (19.5)	26±3 25 (10.5)	23±4 21 (17.5)	20±2 20 (6.5)	19±3 19 (13.5)	21±3 20 (9)	0.66±0.04 0.67 (0.16)	0.80±0.06 0.80 (0.26)	0.86±0.03 0.89 (0.14)	1.02±0.05* 1.00 (0.20)
LV SP, mm Hg	70±5 64 (21)	68±3 67 (13)	61±4 62 (17)	66±8 62 (24)	60±5 65 (20)	62±4 67 (16)	0.86±0.05 0.80 (0.18)	0.92±0.06 0.92 (0.23)	0.99±0.04 0.97 (0.13)	0.97±0.08 1.00 (0.30)
LVEDP, mm Hg	8±1 7 (2.5)	7±1 7 (1.5)	9±1 8 (3.5)	10±1 8 (4.5)	10±1 10 (2.5)	10±1 9 (4)	1.31±0.12 1.29 (0.51)	1.44±0.12 1.38 (0.44)	1.23±0.13 1.13 (0.50)	1.01±0.05 1.00 (0.18)
LV RPP, beats per min×mm Hg/10³	8.2±0.9 8.2 (4.0)	7.1±0.3 7.0 (1.0)	11.3±0.6 11.2 (2.6)	12.1±1.9 10.7 (6.6)	11.4±0.9 12.2 (3.7)	11.8±1.0 13.1 (6.6)	1.42±0.06 1.46 (0.26)	1.65±0.14 1.65 (0.60)	1.01±0.04 1.00 (0.18)	1.02±0.12 0.96 (0.45)
LV DevP, mm Hg	62±5 57 (19)	61±3 60 (12.5)	52±4 55 (16.5)	57±8 54 (23.5)	50±4 56 (18)	53±5 56 (17.5)	0.80±0.05 0.75 (0.18)	0.86±0.08 0.87 (0.30)	0.95±0.04 0.97 (0.14)	0.96±0.08 0.97 (0.32)

Pacing (T2), at the end of the 30-minute hemodynamic stabilization period after the start of pacing. Values are expressed as means±SE and median (interquartile range); n=5 per group. DevP indicates developed pressure; EDP, end-diastolic pressure; HR, heart rate; LV, left ventricular; LVEDP, left ventricular end-diastolic pressure; RPP, rate-pressure product; RV, right ventricular; RVEDP, right ventricular end-diastolic pressure; SP, systolic pressure.

*$P<0.05$ for stress vs dichloroacetate.
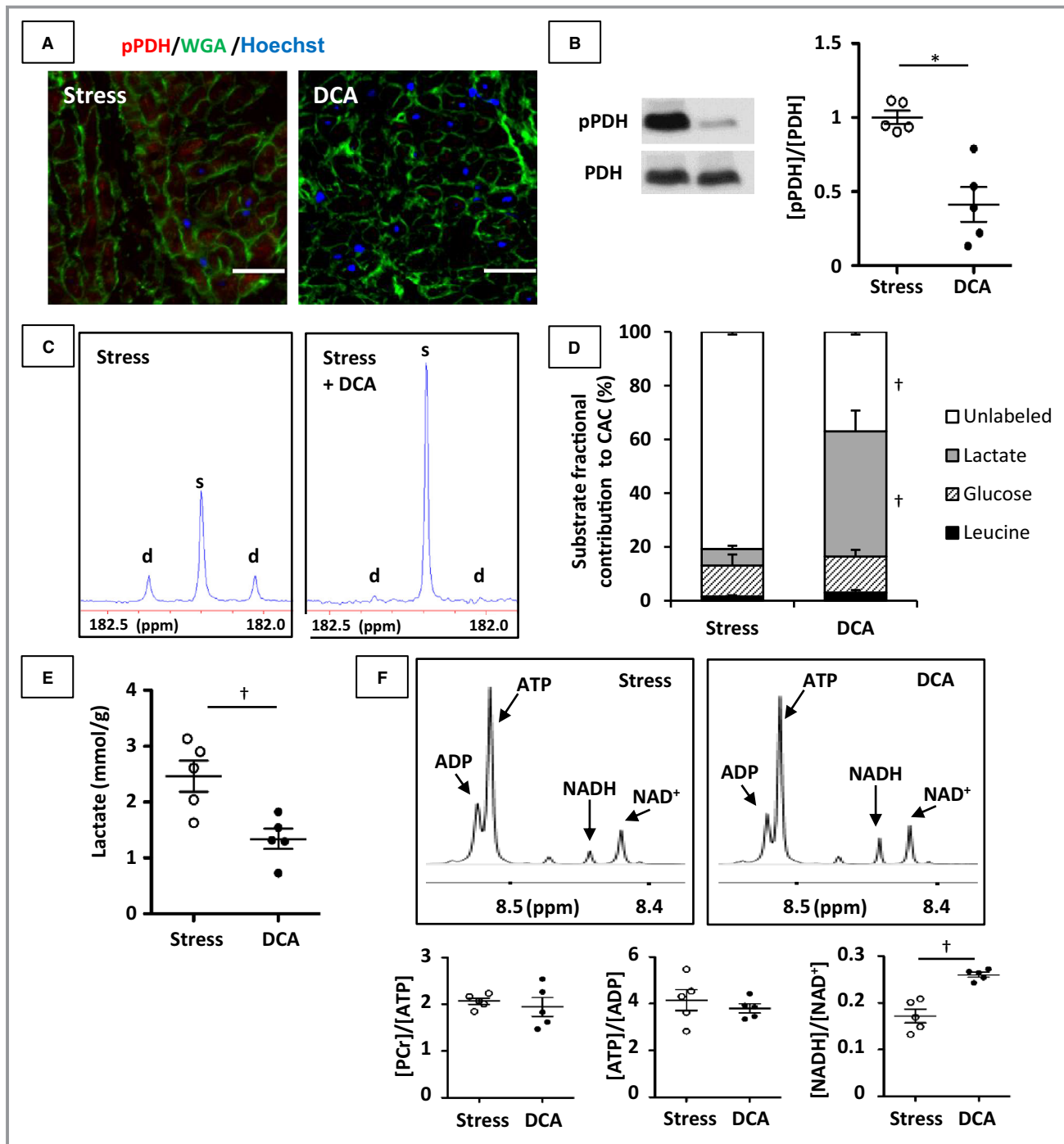
Figure 5. Metabolic alternations by rapid atrial pacing stress and dichloroacetate. **A,** Immunohistochemical staining of phospho-pyruvate dehydrogenase (pPDH). Scale bar: 50 μm. **B,** Representative immunoblots for pPDH/total pyruvate dehydrogenase (PDH), which was detected on the same gel of each protein following reprobing of membranes. Dichloroacetate activated PDH flux (low pPDH, inactive form of PDH). **C,** C5-glutamate in the dichloroacetate group shows prominently increased singlet peak area (s) relative to doublet spike areas (d), indicating increased lactate contribution compared with the stress group. **D,** ^{13}C-nuclear magnetic resonance (NMR) showed that pacing stress limited lactate oxidation and dichloroacetate prominently increased lactate oxidation compared with the stress group. **E,** Gas chromatography mass spectrometry showed that dichloroacetate decreased lactate level in the right ventricle compared with the stress group. **F,** ^{1}H-NMR spectrum for energy metabolites showed that right ventricular[phosphocreatine]/[ATP] and [ATP]/[ADP] were similar between the 2 groups, but dichloroacetate demonstrated significantly higher [nicotinamide adenine dinucleotide (NADH)]/[oxidized form of nicotinamide adenine dinucleotide (NAD^{+})] than the stress group. CAC indicates citric acid cycle; WGA, wheat germ agglutinin. Values are expressed as means±SE; n=5 per group. *$P<0.05$; †$P<0.01$ vs stress.
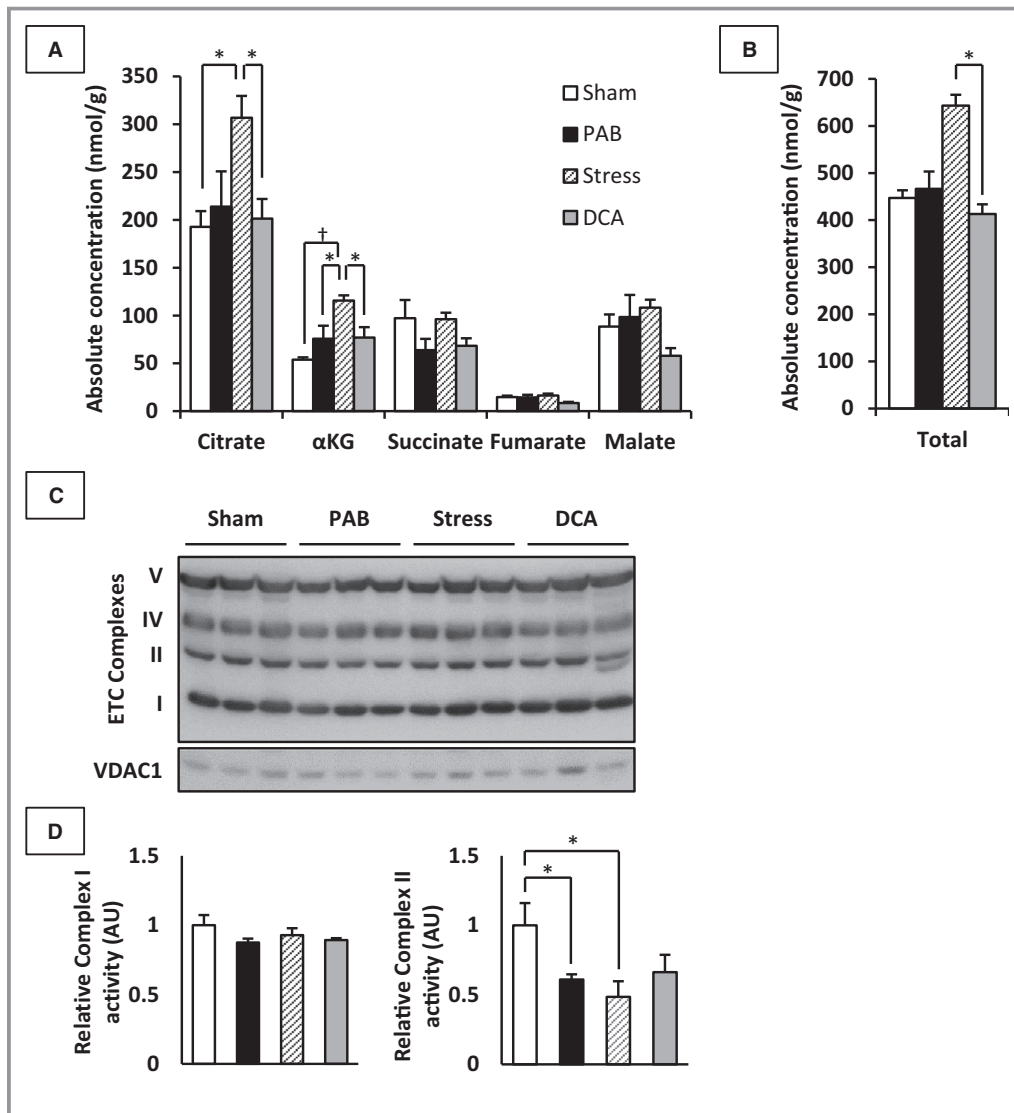
Figure 6. Citric acid cycle (CAC) intermediates concentration and electron transport chain (ETC) enzyme activity in the right ventricle. **A**, Gas chromatography mass spectrometry showed the accumulation of citrate and α-ketoglutarate (αKG) during stress without dichloroacetate compared with the other groups. **B**, Absolute concentration of total CAC intermediates was highest in the stress group among 4 groups. **C**, Protein expression levels of each ETC complex were not different among 4 groups. **D**, ETC complex I and II activities. Chronic right ventricular pressure overload decreased complex II enzyme activity. Acute over pacing stress did not affect mitochondrial ETC I and II enzyme function. AU indicates arbitrary units; PAB, pulmonary artery banding. Values are expressed as means±SE; n=4 to 5 per group. *$P<0.05$; †$P<0.01$.

the inability to substantially increase RPP, a surrogate index for RV myocardial oxygen consumption, suggests that oxidative capacity is limited in the hypertrophied right ventricle. Reduction in oxidative capacity may relate to the fairly low FC for lactate and preference for the oxidation of alternative substrates during the submaximal work increase induced by rapid pacing.

Dichloroacetate blocks PDH kinase inhibitory phosphorylation of the PDH complex. Prior studies,[22] performed in pigs in situ, used dichloroacetate to reveal the relationship between PDH flux and LV functional recovery after transient ischemia

and reperfusion. In those experiments, dichloroacetate infusion into the left anterior descending coronary increased carbohydrate oxidation and prevented both short- and long-term myocardial stunning. Using similar dosing but infused into the right coronary, we found that dichloroacetate markedly decreased PDH phosphorylation, a generally accepted measure of activity state for this enzyme complex. Altering PDH activity by dichloroacetate elevated FC from both lactate and glucose, indicating an increase in PDH flux, while also raising RPP. This enhancement in PDH flux by dichloroacetate produced a greater elevation in RPP and increased PDH flux along with an

increase in [NADH]/[NAD$^+$]. These findings suggest that oxidative capacity is not compromised with the immature hypertrophied right ventricle but that regulation of substrate utilization is altered.

Study Limitations

We used a large animal model in vivo to emulate human neonatal conditions. Therefore, we operated with limitations inherent to performing studies in vivo, and in the right ventricle. As noted in our previous work, the immature right ventricle tolerates only mild PA constriction, and further tightening of the band results in total hemodynamic decompensation. Therefore, we could only use mild PA constriction, which resulted in mild to moderate RV hypertrophy. Possibly, a longer interval would have resulted in gradual band tightening, as occurs clinically with growth, and more extreme hypertrophied right ventricle. Additionally, the venous drainage of the right ventricle through the inaccessible coronary veins precludes accurate measurement of coronary blood return and hence myocardial oxygen consumption. We can only make assumptions for changes in RV myocardial oxygen consumption, which is generally linearly proportional to RPP.[40] The pressure catheters (Millar) provided inconsistent intraventricular pressure rate of rise (dP/dt), as they often imbed in trabecula of the hypertrophied right ventricle. Therefore, we provided RV developed pressure (DevP) as the contractile functional assessment in addition to RPP. The ^{13}C-labeling methods with tcaCALC analyses pose some limitations. FCs can be determined from glutamate-labeling patterns for maximally 3 different substrates. Accordingly, we did not provide ^{13}C-labeled free fatty acids in our infusions. However, fatty acids are supplied from endogenous sources in vivo and are represented in the unlabeled fraction contribution, which is dramatically reduced in PAB under baseline conditions. We presume according to the Randle cycle[41] that the relative increase in carbohydrate oxidation is matched reciprocally by a decrease in fatty acid FC. Sex differences for both cardiac metabolism in newborns and outcomes for congenital heart disease surgeries are now recognized.[42,43] Conceivably, sex differences also exist for the ability of the developing right ventricle to adapt to pressure overload. Only male pigs were used in this study, although examination of sex as a biological factor influencing our results will be an area of future research.

Conclusions

We show that hypertrophy of the immature right ventricle shifts oxidative substrate preference towards substrate entry to the CAC via the PDH pathway to meet contractile energy requirements. However, the immature hypertrophied right ventricle then illustrates an inability to maximally increase

cardiac work abruptly. This limitation can be overcome, at least acutely, by pharmacological disinhibition of PDH by dichloroacetate. Overall, the data suggest that the immature right ventricle undergoes a metabolic maladaptation during hypertrophy, which impairs the ability to increase contractile performance in response to stress. These findings reinforce the potential for metabolic modulation, possibly with dichloroacetate, to improve the function of the immature hypertrophied right ventricle during clinically relevant stress.

Sources of Funding

Disclosures

None.

References

1. Woudstra OI, Ahuja S, Bokma JP, Bouma BJ, Mulder BJM, Christoffels VM. Origins and consequences of congenital heart defects affecting the right ventricle. *Cardiovasc Res*. 2017;113:1509–1520.
2. Roche SL, Redington AN. The failing right ventricle in congenital heart disease. *Can J Cardiol*. 2013;29:768–778.
3. Hayabuchi Y, Sakata M, Kagami S. Right ventricular myocardial deformation patterns in children with congenital heart disease associated with right ventricular pressure overload. *Eur Heart J Cardiovasc Imaging*. 2015;16:890–899.
4. Iacobazzi D, Suleiman MS, Ghorbel M, George SJ, Caputo M, Tulloh RM. Cellular and molecular basis of RV hypertrophy in congenital heart disease. *Heart*. 2016;102:12–17.
5. Reddy S, Bernstein D. Molecular mechanisms of right ventricular failure. *Circulation*. 2015;132:1734–1742.
6. Rain S, Handoko ML, Trip P, Gan CT, Westerhof N, Stienen GJ, Paulus WJ, Ottenheijm CA, Marcus JT, Dorfmuller P, Guignabert C, Humbert M, Macdonald P, Dos Remedios C, Postmus PE, Saripalli C, Hidalgo CG, Granzier HL, Vonk-Noordegraaf A, van der Velden J, de Man FS. Right ventricular diastolic impairment in patients with pulmonary arterial hypertension. *Circulation*. 2013;128:2016–2025, 1–10.
7. Sun XQ, Abbate A, Bogaard HJ. Role of cardiac inflammation in right ventricular failure. *Cardiovasc Res*. 2017;113:1441–1452.
8. Nagendran J, Gurtu V, Fu DZ, Dyck JR, Haromy A, Ross DB, Rebeyka IM, Michelakis ED. A dynamic and chamber-specific mitochondrial remodeling in right ventricular hypertrophy can be therapeutically targeted. *J Thorac Cardiovasc Surg*. 2008;136:168–178, 178.e1-3.
9. Bruns DR, Brown RD, Stenmark KR, Buttrick PM, Walker LA. Mitochondrial integrity in a neonatal bovine model of right ventricular dysfunction. *Am J Physiol Lung Cell Mol Physiol*. 2015;308:L158–L167.
10. Stacpoole PW. The pharmacology of dichloroacetate. *Metabolism*. 1989;38:1124–1144.

11. Kato M, Li J, Chuang JL, Chuang DT. Distinct structural mechanisms for inhibition of pyruvate dehydrogenase kinase isoforms by AZD7545, dichloroacetate, and radicicol. *Structure*. 2007;15:992–1004.

12. Stacpoole PW, Barnes CL, Hurbanis MD, Cannon SL, Kerr DS. Treatment of congenital lactic acidosis with dichloroacetate. *Arch Dis Child*. 1997;77:535–541.

13. Bonnet S, Archer SL, Allalunis-Turner J, Haromy A, Beaulieu C, Thompson R, Lee CT, Lopaschuk GD, Puttagunta L, Bonnet S, Harry G, Hashimoto K, Porter CJ, Andrade MA, Thebaud B, Michelakis ED. A mitochondria-K+ channel axis is suppressed in cancer and its normalization promotes apoptosis and inhibits cancer growth. *Cancer Cell*. 2007;11:37–51.

14. Piao L, Fang YH, Cadete VJ, Wietholt C, Urboniene D, Toth PT, Marsboom G, Zhang HJ, Haber I, Rehman J, Lopaschuk GD, Archer SL. The inhibition of pyruvate dehydrogenase kinase improves impaired cardiac function and electrical remodeling in two models of right ventricular hypertrophy: resuscitating the hibernating right ventricle. *J Mol Med (Berl)*. 2010;88:47–60.

15. Piao L, Sidhu VK, Fang YH, Ryan JJ, Parikh KS, Hong Z, Toth PT, Morrow E, Kutty S, Lopaschuk GD, Archer SL. FOXO1-mediated upregulation of pyruvate dehydrogenase kinase-4 (PDK4) decreases glucose oxidation and impairs right ventricular function in pulmonary hypertension: therapeutic benefits of dichloroacetate. *J Mol Med (Berl)*. 2013;91:333–346.

16. Sun XQ, Zhang R, Zhang HD, Yuan P, Wang XJ, Zhao QH, Wang L, Jiang R, Jan Bogaard H, Jing ZC. Reversal of right ventricular remodeling by dichloroacetate is related to inhibition of mitochondria-dependent apoptosis. *Hypertens Res*. 2016;39:302–311.

17. Kajimoto M, Ledee DR, Isern NG, Portman MA. Right ventricular metabolism during venoarterial extracorporeal membrane oxygenation in immature swine heart in vivo. *Am J Physiol Heart Circ Physiol*. 2017;312:H721–H727.

18. Kajimoto M, Nuri M, Isern NG, Robillard-Frayne I, Des Rosiers C, Portman MA. Metabolic response of the immature right ventricle to acute pressure overloading. *J Am Heart Assoc*. 2018;7:e008570. DOI: 10.1161/JAHA.118.008570

19. Smith AH, Flack EC, Borgman KY, Owen JP, Fish FA, Bichell DP, Kannankeril PJ. A common angiotensin-converting enzyme polymorphism and preoperative angiotensin- converting enzyme inhibition modify risk of tachyarrhythmias after congenital heart surgery. *Heart Rhythm*. 2014;11:637–643.

20. Batra AS, Chun DS, Johnson TR, Maldonado EM, Kashyap BA, Maiers J, Lindblade CL, Rodefeld M, Brown JW, Hubbard JE. A prospective analysis of the incidence and risk factors associated with junctional ectopic tachycardia following surgery for congenital heart disease. *Pediatr Cardiol*. 2006;27:51–55.

21. Rekawek J, Kansy A, Miszczak-Knecht M, Manowska M, Bieganowska K, Brzezinska- Paszke M, Szymaniak E, Turska-Kmiec A, Maruszewski P, Burczynski P, Kawalec W. Risk factors for cardiac arrhythmias in children with congenital heart disease after surgical intervention in the early postoperative period. *J Thorac Cardiovasc Surg*. 2007;133:900–904.

22. Kudej RK, White LT, Kudej AB, Vatner SF, Lewandowski ED. Brief increase in carbohydrate oxidation after reperfusion reverses myocardial stunning in conscious pigs. *Circulation*. 2002;106:2836–2841.

23. Olson AK, Hyyti OM, Cohen GA, Ning XH, Sadilek M, Isern N, Portman MA. Superior cardiac function via anaplerotic pyruvate in the immature swine heart after cardiopulmonary bypass and reperfusion. *Am J Physiol Heart Circ Physiol*. 2008;295:H2315–H2320.

24. Kajimoto M, O'Kelly Priddy CM, Ledee DR, Xu C, Isern N, Olson AK, Portman MA. Extracorporeal membrane oxygenation promotes long chain fatty acid oxidation in the immature swine heart in vivo. *J Mol Cell Cardiol*. 2013;62:144–152.

25. O'Kelly Priddy CM, Kajimoto M, Ledee DR, Bouchard B, Isern N, Olson AK, Des Rosiers C, Portman MA. Myocardial oxidative metabolism and protein synthesis during mechanical circulatory support by extracorporeal membrane oxygenation. *Am J Physiol Heart Circ Physiol*. 2013;304:H406–H414.

26. Comte B, Vincent G, Bouchard B, Jette M, Cordeau S, Des Rosiers C. A 13C mass isotopomer study of anaplerotic pyruvate carboxylation in perfused rat hearts. *J Biol Chem*. 1997;272:26125–26131.

27. Des Rosiers C, Lloyd S, Comte B, Chatham JC. A critical perspective of the use of (13)C-isotopomer analysis by GCMS and NMR as applied to cardiac metabolism. *Metab Eng*. 2004;6:44–58.

28. Kajimoto M, O'Kelly Priddy CM, Ledee DR, Xu C, Isern N, Olson AK, Des Rosiers C, Portman MA. Myocardial reloading after extracorporeal membrane oxygenation alters substrate metabolism while promoting protein synthesis. *J Am Heart Assoc*. 2013;2:e000106. DOI: 10.1161/JAHA.113.000106

29. Kajimoto M, O'Kelly Priddy CM, Ledee DR, Xu C, Isern N, Olson AK, Portman MA. Effects of continuous triiodothyronine infusion on the tricarboxylic acid cycle in the normal immature swine heart under extracorporeal membrane oxygenation in vivo. *Am J Physiol Heart Circ Physiol*. 2014;306:H1164–H1170.

30. Kajimoto M, Ledee DR, Xu C, Kajimoto H, Isern NG, Portman MA. Triiodothyronine activates lactate oxidation without impairing fatty acid oxidation and improves weaning from extracorporeal membrane oxygenation. *Circ J*. 2014;78:2867–2875.

31. Files MD, Kajimoto M, O'Kelly Priddy CM, Ledee DR, Xu C, Des Rosiers C, Isern N, Portman MA. Triiodothyronine facilitates weaning from extracorporeal membrane oxygenation by improved mitochondrial substrate utilization. *J Am Heart Assoc*. 2014;3:e000680. DOI: 10.1161/JAHA.113.000680

32. Kajimoto M, Ledee DR, Olson AK, Isern NG, Des Rosiers C, Portman MA. Differential effects of octanoate and heptanoate on myocardial metabolism during extracorporeal membrane oxygenation in an infant swine model. *Am J Physiol Heart Circ Physiol*. 2015;309:H1157–H1165.

33. Tian R. Transcriptional regulation of energy substrate metabolism in normal and hypertrophied heart. *Curr Hypertens Rep*. 2003;5:454–458.

34. Christe ME, Rodgers RL. Altered glucose and fatty acid oxidation in hearts of the spontaneously hypertensive rat. *J Mol Cell Cardiol*. 1994;26:1371–1375.

35. Taegtmeyer H, Sen S, Vela D. Return to the fetal gene program: a suggested metabolic link to gene expression in the heart. *Ann N Y Acad Sci*. 2010;1188:191–198.

36. Itoi T, Huang L, Lopaschuk GD. Glucose use in neonatal rabbit hearts reperfused after global ischemia. *Am J Physiol*. 1993;265:H427–H433.

37. Ussher JR, Jaswal JS, Lopaschuk GD. Pyridine nucleotide regulation of cardiac intermediary metabolism. *Circ Res*. 2012;111:628–641.

38. Lewandowski ED, O'Donnell JM, Scholz TD, Sorokina N, Buttrick PM. Recruitment of NADH shuttling in pressure–overloaded and hypertrophic rat hearts. *Am J Physiol Cell Physiol*. 2007;292:C1880–C1886.

39. Rupert BE, Segar JL, Schutte BC, Scholz TD. Metabolic adaptation of the hypertrophied heart: role of the malate/aspartate and alpha–glycerophosphate shuttles. *J Mol Cell Cardiol*. 2000;32:2287–2297.

40. Wong YY, Westerhof N, Ruiter G, Lubberink M, Raijmakers P, Knaapen P, Marcus JT, Boonstra A, Lammertsma AA, van der Laarse WJ, Vonk-Noordegraaf A. Systolic pulmonary artery pressure and heart rate are main determinants of oxygen consumption in the right ventricular myocardium of patients with idiopathic pulmonary arterial hypertension. *Eur J Heart Fail*. 2011;13:1290–1295.

41. Randle PJ, Garland PB, Hales CN, Newsholme EA. The glucose fatty-acid cycle. Its role in insulin sensitivity and the metabolic disturbances of diabetes mellitus. *Lancet*. 1963;1:785–789.

42. Kochilas LK, Vinocur JM, Menk JS. Age-dependent sex effects on outcomes after pediatric cardiac surgery. *J Am Heart Assoc*. 2014;3:e000608. DOI: 10.1161/JAHA.113.000608

43. Wittnich C, Quaglietta D, Tan L, Belanger MP. Sex differences in newborn myocardial metabolism and response to ischemia. *Pediatr Res*. 2011;70:148–152.

SUPPLEMENTAL MATERIAL

Data S1.

Supplemental Methods

A pig model of chronic RV pressure overload. Pigs were initially sedated with an intramuscular injection of ketamine (33 mg/kg) and xylazine (2 mg/kg) and were placed on a circulating warming blanket for keeping a rectal temperature of 36-37.5°C. Pigs were intubated with an endotracheal tube, facilitating mechanical ventilation and general anesthesia under inhaled isoflurane (1-3%) with oxygen (40-50%). Monitors were placed for electrocardiogram, pulse oximetry, and rectal temperature. A PowerLab 16/30 recorder (AD Instruments, Colorado Springs, CO) was used to continuously record hemodynamic data throughout the surgical procedure. Pigs were placed on right lateral position. Surgical skin preparation with povidone-iodine and an iodine-containing incise drape were applied to the left lateral chest. Bupivacaine (0.25% 1 mL/kg) was administered locally to the skin incision intercostal area for a left lateral thoracotomy. Heart and pulmonary artery (PA) were exposed through a small left lateral thoracotomy in the 4th or 5th intercostal space and partial pericardiotomy, and 2 pressure catheters (Millar Instruments, Houston, TX) were sited into the RV and ascending aorta directly through RV free wall and the aortic wall respectively. Baseline hemodynamic and blood measurements were made. The main PA was carefully dissected from the ascending aorta, and then banding tape was placed around the main PA using a cotton umbilical tape ~3 mm width (Ethicon, Somerville, NJ). In Sham group, the banding tape was just looped around the PA without constriction. In experimental (PAB) group, the banding tape was gradually constricted to increase two-fold of the baseline RV systolic pressure. Postoperative analgesia with fentanyl patch (3-5 µg/kg/hour), buprenorphine (0.01 mg/kg every 12 hours) and ketoprofen (2 mg/kg every 24 hours) was administered for at least 72 hours. Animals were housed in a caged facility with full access to feed and water. A direct echocardiograms and Doppler studies on the epicardium were performed for measurement of cardiac function, RV free wall thickness

(RVWT) and PA flow using an ultrasound machine, Sequoia C256 (Siemens) at baseline prior to PAB, and then again at 7 to 10 days after the initial procedure. M-Mode measurements were obtained at end-diastole for determination of RVWT. The pulsed Doppler velocity was measured across the PAB site. This velocity serves as a standard non-invasive estimate of the peak instantaneous pressure gradient across the band site and is calculated by the modified Bernoulli equation (Δ pressure gradient = $4*velocity^2$).[1] The metabolic analysis was performed at 7 to 10 days after the 1st procedure (PAB or Sham procedure). For protocol 2, increase cardiac workload by rapid atrial pacing and sodium dichloroacetate (DCA) supplement were performed, and were followed by metabolic analysis.

Increase cardiac workload by rapid atrial pacing and DCA supplement. Protocol 2 was performed with atrial over pacing and DCA supplement at 2nd operation. Pigs were initially sedated with an intramuscular injection of ketamine (33 mg/kg) and xylazine (2 mg/kg) and were placed on a circulating warming blanket for keeping a rectal temperature of 36-37.5°C. After intubation through a surgical tracheostomy, the pigs were mechanically ventilated with oxygen (40-50%) and isoflurane (1-3%) mixture in a monitored setting of electrocardiogram and oxygen saturation. Angio catheters were inserted into the right femoral artery and central vein through the left external jugular vein for continuous recording of the pressure, fluid infusion and blood sample. After median sternotomy, a flow probe (Transonic Systems Inc, Ithaca, NY) around ascending aorta was attached, and both ventricular pressure catheters (Millar Instruments, Houston, TX) and pulmonary artery (PA) pressure catheter (24-gauge angio catheter) were directly inserted. After opening the pericardium, two epicardial pacing electrodes were placed into the right atrial myocardium and were connected to an external temporary dual-chamber pulse generator (Medtronic model 5345; Minneapolis, Minnesota). Increase cardiac workload was induced by rapid right atrial pacing at a rate of ~80% increase in baseline heart rate. After around 30 minutes hemodynamic stabilization, DCA, obtained from Sigma-Aldrich (St. Louis,

MO, catalog # 347795), was infused through the right coronary artery. Study group was 2 with DCA (n = 5) or phosphate-buffered saline (n = 5) administered for 60 minutes. Target intracoronary concentration of DCA was adjusted to 4 mM. This concentration of DCA use in our study is well within the range used by other investigators and based on the estimation method of Kudej used in adult pig coronary ischemia model.[2]

Metabolic analysis. The metabolic analysis was performed at 7-10 days after the 1st procedure (PAB or sham procedure). Carbon 13 (^{13}C)-labeled substrates were used as metabolic tracers. [2-^{13}C]lactate (catalog # 589209)and [U-^{13}C$_6$]leucine (catalog # 608068) were obtained from Sigma-Aldrich, and [1-^{13}C]glucose (catalog # CLM-3612) was obtained from Cambridge Isotope Laboratories (Andover, MA). After appropriate sedation and anesthesia, the pigs were intubated through a surgical tracheostomy and were mechanically ventilated with oxygen (40-50%) and isoflurane (1-3%) mixture in a monitored setting of electrocardiogram and oxygen saturation. Angio catheters were inserted into the right femoral artery and central vein through the left external jugular vein for continuous recording of the pressure, fluid infusion and blood sample. Arterial blood glucose, pH, PCO_2, PO_2, and hemoglobin were measured at regular intervals until the end of the experiment by Radiometer ABL 800 (Radiometer America, Westlake, OH). Plasma triglyceride level was also measured using commercial kits (Cayman, Ann Arbor, MI, USA, catalogue # 10010303). After median sternotomy, both ventricular pressure catheters (Millar Instruments, Houston, TX) and pulmonary artery (PA) pressure catheter (24-gauge angio catheter) were directly inserted. Labeled substrates in all protocols were infused from the right coronary artery through a directly inserted 24-gauge angio catheter for the final 60 minutes of the protocol. The intracoronary doses were adjusted to achieve 1.2 mM [2-^{13}C]lactate, 2 mM [1-^{13}C]glucose and 2 mM [U-^{13}C$_6$]leucine elevations in the right coronary artery and were based upon the mean coronary artery flow per body weight calculated in our preliminary pig experiments.[3-5] Freeze-clamped sections of RV in the region perfused by

the right coronary artery were pulverized under liquid nitrogen and were stored at -80 °C for further metabolic studies.

Preparation of myocardial extracts. Tissue processing was previously described.[5, 6] Briefly, freeze-clamped RV tissues were ground into fine powder under liquid nitrogen. The tissue was extracted with either methanol/chloroform or 1.2 M perchloric acid, then neutralized with cold KOH to pH 7.4. The final supernatant was lyophilized overnight at -50 °C. The lyophilized product was utilized for mass spectrophotometry or ^{13}C-Nuclear Magnetic Resonance (NMR) spectral acquisition.

Nuclear Magnetic Resonance (NMR). ^{13}C- and ^{1}H-NMR were performed on the RV extract tissue for measuring the fractional contribution (Fc) of each substrate to the acetyl coenzyme A (acetyl-CoA) pool entering the citric acid cycle (CAC) and for measuring the concentration of myocardial energy metabolites respectively as previously described.[4, 5, 7-11] ^{13}C-NMR allows determination of the fractional contribution of labeled substrates via analyses of the ^{13}C-glutamate spectrum. ^{1}H-NMR permits well validated high resolution and high sensitivity analyses for quantitation of a robust number of metabolites including high-energy phosphates, such as phosphocreatine (PCr), adenosine triphosphate (ATP), adenosine diphosphate (ADP), and nicotinamide adenine dinucleotide (NADH).[12]

Freeze-clamped hearts were ground into fine powder under liquid nitrogen and 0.5 mg further homogenized in 2.5 ml of a methanol/ddH$_2$O (1:0.25) mix. A 2:1 chloroform/ddH$_2$O mix was added to the homogenate, vortexed, and placed on ice for 10 minutes. The samples were next centrifuged for 10 minutes at 2000 g. The top layer was removed to a fresh tube and subjected to vacuum lyophilization. The resulting precipitate was dissolved in deuterium oxide (DLM11-100, Cambridge Isotopes, Andover, MA) and Chenomx ISTD (IS-1, Chenomx, Alberta Canada) at a 9:1 ratio, filtered through a 0.22 µM syringe filter into NMR sample tubes (WG-1241-8, Wilmad LabGlass, Vineland, NJ). ^{13}C-NMR data were acquired on a Varian Direct Drive (VNMRS) 600 MHz spectrometer (Agilent Technologies) equipped with a Dell Precision T3500

Linux workstation running VNMRJ 4.0. The spectrometer system was outfitted with a Varian triple resonance salt-tolerant cold probe with a cold carbon preamplifier. Fourier-transformed spectra were fitted with commercial software (NUTS, Acorn NMR Inc., Livermore, CA), and then the data, which determined from specific carbon glutamate labeling was analyzed by the CAC analysis-fitting algorithm tcaCALC (kindly provided by the Advanced Imaging Research Center at the University of Texas, Southwestern). A Varian standard one dimensional proton noesy with presaturation (tnnoesy) was collected on each sample, using a nonselective 90 degree excitation pulse (approximately 7 μs at 57 dB), a 100 ms mixing time, acquisition time of 4 seconds, a presaturation delay of 1.5 seconds, spectral width of 12 parts-per-million (ppm), and temperature control set to 25 °C. Collected spectra by ^{1}H-NMR were analyzed using Chenomx software (version 8.3, Chenomx) with quantifications based on spectral intensities relative to 0.5 mM 2,2-dimethyl-2-silapentane-5-sulfonate (DSS), which was added as a spike to each sample. Values were normalized relative to total creatine.

Energy metabolites in RV tissue were measured by ^{1}H-NMR. Chemical shifts of ^{1}H-NMR resonance peaks on energy metabolites were creatine (Cr, 3.022 and 3.915 ppm); PCr (3.028 and 3.935 ppm); adenosine diphosphate (ADP, 4.204, 4.247, 4.370, 4.592, 6.135, 8.251, 8.524 ppm); ATP (4.230, 4.275, 4.400, 4.566, 6.136, 8.254, 8.514 ppm); the reduced form of NAD (NADH, 4.696, 5.976, 6.932, 8.443 ppm); the oxidized form of NAD (NAD$^+$, 4.535, 6.030, 6.073, 8.160, 8.184, 8.420, 8.822, 9.139, 9.325 ppm); the reduced form of NADP (NADPH, 4.972, 5.965, 6.195, 6.616, 6.956, 8.235, 8.472 ppm); the oxidized form of NADP (NADP$^+$, 4.975, 6.042, 8.132, 8.180, 8.406, 8.808, 9.098, 9.280 ppm) relative to the DSS peak.

Gas chromatography-mass spectrometry (GCMS). GCMS was performed to measure the concentrations of CAC intermediates (citrate, α-ketoglutarate, succinate, fumarate and malate), pyruvate, lactate, and glutamate in RV tissue using Agilent 6890N gas chromatograph equipped with a HP-5 column coupled to a 5975N mass spectrometer (Agilent Technologies, Santa Clara, CA) as described elsewhere.[7]

Western Blot Analysis. The primary antibodies (the list of the antibodies is provided in below **Table S1**) used in this study were 5' adenosine monophosphate-activated protein kinase α (AMPKα), phospho-AMPKα-Thr172, acetyl-CoA carboxylase (ACC), phospho-ACC-Ser79 and PDH obtained from Cell Signaling Technology (Danvers, MA), and phospho-PDH-Ser293 obtained from Millipore (Billerica, MA). Fifty micrograms of total protein extract from RV were heated at 95 °C for 5 min and were electrophoresed through 4.5% stacking and 10% running SDS-polyacrylamide gels and electroblotted onto polyvinylidene difluoride (PVDF)-plus membranes. Equal protein loading of samples was determined by a protein assay (BioRad, Hercules, CA) and confirmed by reversible protein stain kit for PVDF membranes (Thermo Scientific, Rockford, IL). Membranes were probed overnight at 4 °C with primary antibodies (phospho-PDH, phospho-ACC and phospho-AMPKα) dissolved in Tris-Buffered Saline and Tween 20 (TBST) containing 5% milk or bovine serum albumin. Blots were incubated at room temperature for 1 hour with the appropriate secondary antibody conjugated to horseradish peroxidase. The blots were visualized with enhanced chemiluminescence after exposure to X-ray film. The densitometric intensities were determined using Image J analysis software (National Institutes of Health, Bethesda, MD). Probes were stripped off the membranes upon incubation in Restore Western Blot Stripping Buffer (Thermo Scientific, catalogue #21059) at room temperature, and the membranes were reprobed with antibodies against PDH, ACC, AMPKα and the loading control, α-Tubulin (Santa Cruz Biotechnology, Santa Cruz, CA).

Histology. The fresh frozen RV free wall tissues were embedded in OCT compound in cryomolds. They were sectioned using a cryostat into 5-μm-thick slices, mounted onto slides, and then fixed in acetone. Wheat germ agglutinin (WGA) staining was performed to measure cell size. Slides were stained for 10 min with Alexa Fluor 488-conjugated WGA (1:200, Invitrogen, Carlsbad, CA) and Hoechst 33342 (1:1000, Invitrogen) at room temperature. Images were obtained using a digital fluorescence microscope (BZ-X700, Keyence, Osaka, Japan) at a 20x objective lens magnification and were analyzed by image software, Fiji (an open source

imaging program). The outline of myocytes was traced to determine myocyte cross-sectional area. A value was calculated by the measurements of 200 cells (from 3 non-overlapping images randomly chosen for each slide) in an individual heart (2 slides for each animal). For the assessment of the extent of total myocardial fibrosis, slides were stained with Masson's trichrome (Polysciences Inc., Warrington, PA) according to a standard protocol. Sections were incubated in bouins (overnight), weigert's iron hematoxylin (10 min), biebrich scarlet-acid fuchsin (5 min), phosphotungstic/phosphomolybdic Acid (10 min), aniline blue (5 min) and 1% acetic acid (1 min) in order. In this staining, cytoplasm and muscle fibers stain red whereas collagen fibers display blue coloration. Slide images were obtained using a digital microscope (BZ-X700, Keyence) at a 4x objective lens magnification. Six non-overlapping images were randomly chosen for analysis of each animal, and total myocardial fibrosis percentage was adjusted to a total tissue area in the analyzed image by Fiji. Phospho-PDH-E1α-Ser293 (1:500) was also used for immunohistochemical staining with WGA to confirm the activation effect of DCA to PDH flux. Donkey anti-rabbit Alexa Fluor 546 (Invitrogen, catalogue # A10040) was used as the secondary antibody.

ETC complexes assembly immunoblotting. ETC complexes assembly was assessed by using the total oxidative phosphorylation (OXPHOS) rodent WB antibody cocktail (abcam, catalogue # ab110413) that included specific subunit of each of the five ETC complexes. After protein extraction from fresh frozen RV, fifty micrograms of total protein extract from RV were heated at 50 °C for 5 min and were electrophoresed through 4.5% stacking and 12% running SDS-polyacrylamide gels and electroblotted onto PVDF membranes. The membrane was then blocked overnight with TBST-5% milk. They were probed with 6.0 µg/mL (dilution 1:250) of antibodies cocktail overnight at 4°C, and then incubated with secondary antibody anti-mouse horseradish peroxidase-conjugated for 1 hour. The blots were visualized with enhanced chemiluminescence after exposure to X-ray film. The densitometric intensities were determined using Image J analysis software (National Institutes of Health, Bethesda, MD). Equal protein

loading of samples was determined by a protein assay (BioRad, Hercules, CA) and confirmed by reversible protein stain kit for PVDF membranes (Thermo Fisher Scientific, Rockford, IL) as well as the loading control, voltage-dependent anion-selective channel 1 (VDAC1).

Mitochondrial Electron Chain Transport (ETC) enzyme activity. Enzymatic activities of the mitochondrial ETC complex I and II in the RV were assessed using commercially available assay kits (Cayman, catalogue # 700930 and 700940) according to the manufacturer's instruction. The activity of complex I was assessed by the reduction rate of NADH oxidation in absorbance at 340 nm (**Figure S1A**). The activity of complex II was assessed by the reduction rate of 2,6-dichlorophenol-indophenol (DCPIP) in absorbance at 600 nm (**Figure S1B**). For these reaction assays, 2 µg isolated mitochondrial protein from the fresh frozen RV free wall tissues was loaded. Isolation of cardiac mitochondria was used by commercially available kits (Thermo Fisher Scientific, catalogue # 89801) according to manufacturer's instruction.

Table S1. Antibodies.

Antibodies	Supplier	Dilution	Reference
ACC	Cell Signaling Technology	1:1,000	3676
AMPKα	Cell Signaling Technology	1:1,000	5831
OXPHOS	abcam	1:250	ab110413
PDH	Cell Signaling Technology	1:1,000	2784
Phospho-ACC	Cell Signaling Technology	1:1,000	3661
Phospho-AMPKα	Cell Signaling Technology	1:1,000	2535
Phospho-PDH-E1α	Millipore	1:10,000 for WB 1:500 for IHC	ABS204
α-Tubulin	Santa Cruz Biotechnology	1:20,000	sc-12462-R
VDAC1	Santa Cruz Biotechnology	1:1,000	sc-8829
Labeling solutions			
Hoechst 33342	Invitrogen	1:1,000	H1339
WGA, Alexa Fluor 488 Conjugate	Invitrogen	1:200	W11261

Figure S1. Mitochondrial ETC enzyme activities for complex I and II in RV.
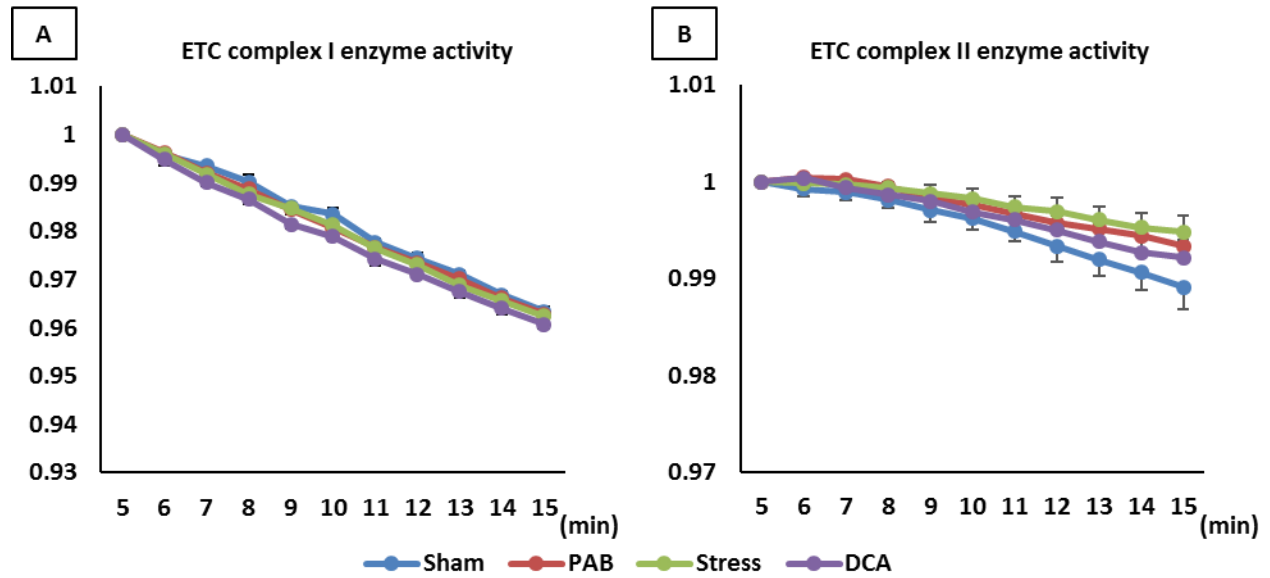
The activity of complex I and II were assessed by the reduction rate of NADH oxidation and 2,6-dichlorophenol-indophenol respectively. RV pressure overload decreased mitochondrial ETC complex II enzyme activity.

Supplemental References:

1.   Valdes-Cruz LM, Horowitz S, Sahn DJ, Larson D, Oliveira Lima C and Mesel E. Validation of a Doppler echocardiographic method for calculating severity of discrete stenotic obstructions in a canine preparation with a pulmonary arterial band. *Circulation*. 1984;69:1177-81.

2.   Kudej RK, White LT, Kudej AB, Vatner SF and Lewandowski ED. Brief increase in carbohydrate oxidation after reperfusion reverses myocardial stunning in conscious pigs. *Circulation*. 2002;106:2836-41.

3.   Olson AK, Hyyti OM, Cohen GA, Ning XH, Sadilek M, Isern N and Portman MA. Superior cardiac function via anaplerotic pyruvate in the immature swine heart after cardiopulmonary bypass and reperfusion. *Am J Physiol Heart Circ Physiol*. 2008;295:H2315-20.

4.   Kajimoto M, O'Kelly Priddy CM, Ledee DR, Xu C, Isern N, Olson AK and Portman MA. Extracorporeal membrane oxygenation promotes long chain fatty acid oxidation in the immature swine heart in vivo. *J Mol Cell Cardiol*. 2013;62:144-52.

5.   O'Kelly Priddy CM, Kajimoto M, Ledee DR, Bouchard B, Isern N, Olson AK, Des Rosiers C and Portman MA. Myocardial oxidative metabolism and protein synthesis during mechanical circulatory support by extracorporeal membrane oxygenation. *Am J Physiol Heart Circ Physiol*. 2013;304:H406-14.

6.   Comte B, Vincent G, Bouchard B, Jette M, Cordeau S and Rosiers CD. A 13C mass isotopomer study of anaplerotic pyruvate carboxylation in perfused rat hearts. *J Biol Chem*. 1997;272:26125-31.

7.   Des Rosiers C, Lloyd S, Comte B and Chatham JC. A critical perspective of the use of (13)C-isotopomer analysis by GCMS and NMR as applied to cardiac metabolism. *Metab Eng*. 2004;6:44-58.

8.   Kajimoto M, O'Kelly Priddy CM, Ledee DR, Xu C, Isern N, Olson AK, Des Rosiers C and Portman MA. Myocardial reloading after extracorporeal membrane oxygenation alters substrate metabolism while promoting protein synthesis. *J Am Heart Assoc*. 2013;2:e000106.

9.   Kajimoto M, O'Kelly Priddy CM, Ledee DR, Xu C, Isern N, Olson AK and Portman MA. Effects of continuous triiodothyronine infusion on the tricarboxylic acid cycle in the normal immature swine heart under extracorporeal membrane oxygenation in vivo. *Am J Physiol Heart Circ Physiol*. 2014;306:H1164-70.

10.   Files MD, Kajimoto M, O'Kelly Priddy CM, Ledee DR, Xu C, Des Rosiers C, Isern N and Portman MA. Triiodothyronine facilitates weaning from extracorporeal membrane oxygenation by improved mitochondrial substrate utilization. *J Am Heart Assoc*. 2014;3:e000680.

11.   Kajimoto M, Ledee DR, Xu C, Kajimoto H, Isern NG and Portman MA. Triiodothyronine activates lactate oxidation without impairing Fatty Acid oxidation and improves weaning from extracorporeal membrane oxygenation. *Circ J*. 2014;78:2867-75.

12.   Chen JH, Wu YV, DeCarolis P, O'Connor R, Somberg CJ and Singer S. Resolution of creatine and phosphocreatine 1H signals in isolated human skeletal muscle using HR-MAS 1H NMR. *Magn Reson Med*. 2008;59:1221-4.